A fast semi-analytical method for propagating leaky Lamb wavefields

Håvard Kjellmo Arnestad[1], Erlend Magnus Viggen[2]

[1] Department of Physics, Norwegian University of Science and Technology
[2] Centre for Innovative Ultrasound Solutions, Department of Circulation and Medical Imaging, Norwegian University of Science and Technology
Contact email: havard.arnestad@gmail.com

Abstract

A fast method is presented for calculating the wavefields from initialized leaky Lamb waves on plates immersed in sufficiently light fluids. The method works by precomputing the dispersion relation and attenuation, and propagating the wavefields in the frequency domain. An angular spectrum approach is used to include leakage into surrounding fluid. Compared to matching FEM simulations, the computations are performed in the order of seconds, rather than hours. The method also benefits from being much easier to set up correctly, but is on the other hand less general in that it cannot handle e.g. scattering from defects. The correspondence is shown to be good for the case of interest.

1 Introduction

Due its simple geometry, plates and plate-like structures are often encountered in nature as well as in the man-made world. The examples range from the ice on a frozen lake to the hull of a ship, or the casings in an oil well. In situations where such systems are to be probed, acoustic methods are often chosen due to being relatively non-invasive. The methods rely on different principles, but can be broadly categorized into response and modal methods [1]. In response methods, one studies the response from a known excitation, using e.g. reflection coefficients, and in modal methods, one studies the propagation characteristics, such as attenuation or propagation speed. For a plate with a specified initial wavefield, the modal approach is the only feasible option.

The propagation properties of acoustic waves in plates are described by Lamb wave theory, which is a special case of elastic waves in layered media, with only a single layer in a vacuum. In most practical situations, however, the plate is in contact with a fluid on one or both sides, making it "leaky" in the sense that the plate wave is attenuated as waves are radiated into the surrounding medium. The radiation makes fluid-immersed transducers suitable for measuring the radiated wavefront from e.g. a wavepacket propagating on the plate, as is done in pitch-catch well logging [2–5].

Full simulation of ultrasonic plate waves in e.g. COMSOL Multiphysics can be very slow as the domain must be finely meshed. Proper initialization of wave packets is also more complicated than one first may think, because multiple fields must be correctly set up at all relevant frequencies.

ISBN 978-82-8123-021-7

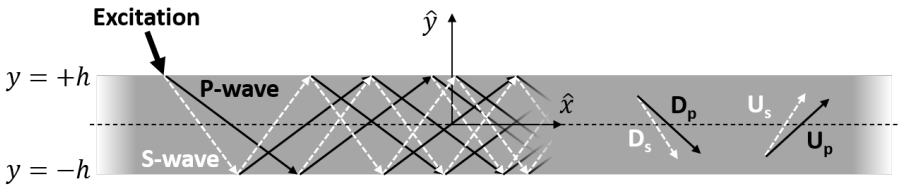

Figure 1: Schematic development of a Lamb wave. D_p, D_s, U_p and U_s represent a steady pattern of P- and S-waves traveling upwards and downwards in the plate. There is vacuum outside the plate boundaries at $y = \pm h$.

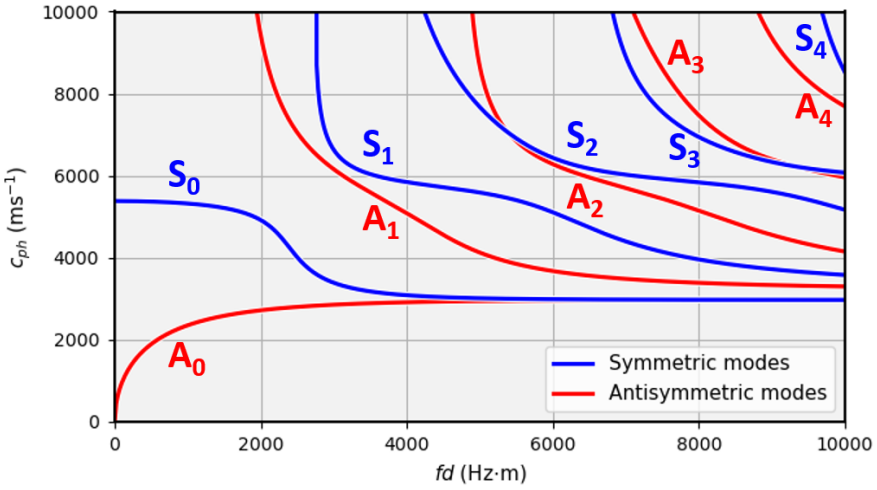

Figure 2: Phase velocities for Lamb modes in a generic steel plate as a function of the frequency-thickness product fd, where $d = 2h$ is the thickness of the plate.

Faster simulation can be achieved by exploiting that the propagation characteristics are already known from modal Lamb wave analysis, as will be presented in this article. The semi-analytical method presented here uses a Fourier decomposition of the wavefield for each mode, where propagation is achieved by adjusting the phase of the mode according to its dispersion relation. Radiation into the surrounding fluid medium is implemented using an angular spectrum approach, relying directly on the aforementioned Fourier decomposition. Attenuation is included using a perturbation-based method valid for light fluids (i.e., with a much lower density than that of the plate).

2 Theory

2.1 Lamb wave theory

Lamb waves are the modal solution of guided waves in a free plate. Consider Fig. 1, which represents a slab of elastic media such as steel. As the plate is excited, waves are reflected from the two free boundaries. Any propagating wavemodes must eventually create a steady pattern of plane waves which leads to different propagating modes that are symmetric (S_0, S_1, etc.) or antisymmetric (A_0, A_1, etc.) with respect to the midplane of the plate. Examples of possible phase and group velocities for these modes are shown in Fig. 2 and 3. To understand how these modes come to be, first consider that two types of waves can be supported in an elastic plate: longitudinal P-waves (for primary/pressure),

ISBN 978-82-8123-021-7

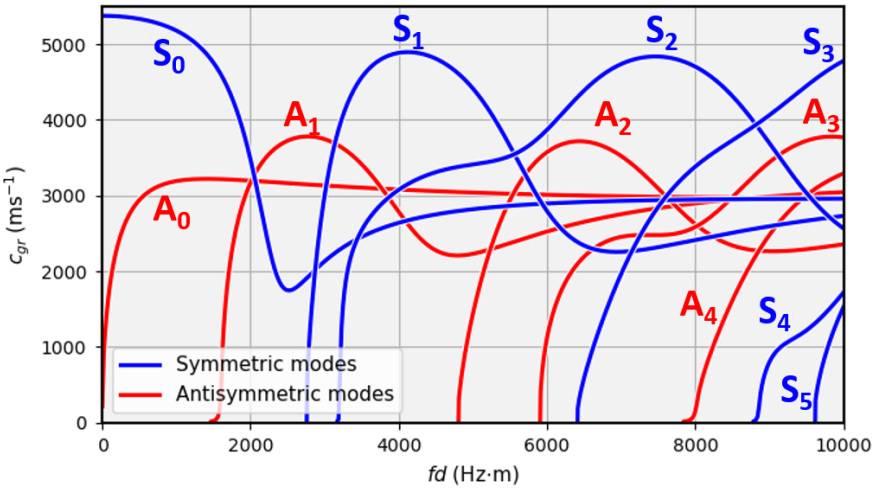

Figure 3: Group velocities for a steel plate as a function of the frequency-thickness product fd.

and transversal S-waves (for secondary/shear), with sound speeds given by

$$c_p = \sqrt{\frac{\lambda + 2G}{\rho}}, \tag{1a}$$

$$c_s = \sqrt{\frac{G}{\rho}}. \tag{1b}$$

Here, λ and G are the first and second Lamé constants that define the stress-strain relationship in isotropic media, and ρ is the density. The Lamé constants can be expressed from the more experimentally available Young's modulus E and Poisson's ratio ν as

$$\lambda = \frac{\nu E}{(1+\nu)(1-2\nu)}, \tag{2a}$$

$$G = \frac{E}{2(1+\nu)}. \tag{2b}$$

The general displacement field $\boldsymbol{u}$ can be written using Helmholtz decomposition theorem from the scalar (ϕ) and vector ($\boldsymbol{\Psi}$) wave potentials as

$$\boldsymbol{u} = \nabla\phi + \nabla \times \boldsymbol{\Psi} = \boldsymbol{u}_p + \boldsymbol{u}_s. \tag{3}$$

A solution is sought in the x-y plane, where the fields are invariant in the z-direction. It can be shown that the u_z-components depends only on the potentials Ψ_x and Ψ_y that are associated with the horizontally polarised shear wave (SH). The other two components depend on potentials ϕ and $\Psi_z = \psi$, associated with longitudinal waves (P) and vertically polarised shear waves (SV), respectively. It is therefore possible to seek solutions separately for the P + SV wave combination. In the remaining analysis the SH waves are discarded because they do not couple to a fluid.

In a solid layer, the fields of a right-going wave may thus be expressed as the superposition of four plane waves. These are the P- and SV-waves (from here on abbreviated as S) propagating in the upwards and downwards directions. Snell's law requires that the wave vectors are oriented so that they all have the same component β, equal to k_x in this situation, along the waveguide propagation direction. That implies the concept

ISBN 978-82-8123-021-7

of transverse resonance for plates; with lossless boundaries, the mode solutions are traveling along the waveguide axis and are standing waves in the transverse direction. The potentials from these four plane waves can be written as

$$\phi = \left[D_p e^{i\gamma_p y} + U_p e^{-i\gamma_p y}\right] e^{i(\omega t - \beta x)}, \tag{4a}$$

$$\psi = \left[D_s e^{i\gamma_s y} + U_s e^{-i\gamma_s y}\right] e^{i(\omega t - \beta x)}, \tag{4b}$$

where D_p and D_s are the wave potential amplitudes of downward-moving P- and S-waves respectively, and U_p and U_s are the amplitudes of upwards-moving waves. The horizontal wavenumbers β are the same for all the plane waves, as mentioned. Because of the different wave speeds, the wavenumbers of P- and S-waves differ: $k_p = \omega/c_p$ and $k_s = \omega/c_s$. The vertical wavenumbers k_y, are therefore also different for P- and S-waves, and are denoted by γ_p and γ_s respectively:

$$\gamma_s = \sqrt{k_s^2 - \beta^2}, \tag{5a}$$

$$\gamma_p = \sqrt{k_p^2 - \beta^2}. \tag{5b}$$

The real power of the formulation emerges when introducing the field variables as expressed via the four wave components. Naturally, when two layers are in contact, the boundary conditions need to be matched. For elastic waves that means the continuity of particle displacement, and normal and shear stress (σ_{yy} and σ_{xy}). One can obtain expressions for the stresses by calculating the strain from particle displacement, and then pipe the result into the constitutive relation for stress, which is where the Lamé constants are introduced. As can be verified with a textbook on the matter [6, 7], one obtains

$$\sigma_{xx} = \lambda\left(\frac{\partial^2\phi}{\partial x^2} + \frac{\partial^2\phi}{\partial y^2}\right) + 2G\left(\frac{\partial^2\phi}{\partial x^2} + \frac{\partial^2\psi}{\partial x\partial y}\right), \tag{6a}$$

$$\sigma_{xy} = G\left(2\frac{\partial^2\phi}{\partial x\partial y} - \frac{\partial^2\psi}{\partial x^2} + \frac{\partial^2\psi}{\partial y^2}\right), \tag{6b}$$

$$\sigma_{yy} = \lambda\left(\frac{\partial^2\phi}{\partial x^2} + \frac{\partial^2\phi}{\partial y^2}\right) + 2G\left(\frac{\partial^2\phi}{\partial y^2} - \frac{\partial^2\psi}{\partial x\partial y}\right). \tag{6c}$$

Any stress component with a z-index is zero, and although σ_{xx} is not an imposed boundary condition, it will be needed in a later section. The last step is to substitute the plane wave formulation of the potentials into the stress and displacement equations. A bit of rearrangement yields a matrix equation for the stress and displacement through the plane wave amplitudes in $y = 0$, which is an arbitrary origin.

$$\begin{bmatrix} \sigma_{yy}(y) \\ \sigma_{xy}(y) \\ u_y(y) \\ u_x(y) \end{bmatrix} = \begin{bmatrix} G(\beta^2 - \gamma_s^2) & G(\beta^2 - \gamma_s^2) & -2G\beta\gamma_s & 2G\beta\gamma_s \\ 2G\beta\gamma_p & -2G\beta\gamma_p & G(\beta^2 - \gamma_s^2) & G(\beta^2 - \gamma_s^2) \\ i\gamma_p & -i\gamma_p & i\beta & i\beta \\ -i\beta & -i\beta & i\gamma_s & -i\gamma_s \end{bmatrix} \begin{bmatrix} D_p e^{+i\gamma_p y} \\ U_p e^{-i\gamma_p y} \\ D_s e^{+i\gamma_s y} \\ U_s e^{-i\gamma_p y} \end{bmatrix}. \tag{7}$$

Similar matrices using a different coordinate convention can be found from e.g. Hovem [7] or Lohne et al. [8]. Using a matrix formulation gives a systematic way of working with guided waves in multi-layered media, such as plates in contact with different fluids or solids. Here we limit ourselves to free plates and will not go into more details or generalizations than needed.

ISBN 978-82-8123-021-7

The plate considered is a single layer with with thickness $d = 2h$, and boundaries to vacuum at $y = \pm h$. The vacuum boundary conditions require that the relevant stresses are zero. Evaluated with respect to the mid-plane of the plate,

$$\begin{bmatrix} \sigma_{yy}(+h) \\ \sigma_{xy}(+h) \\ \sigma_{yy}(-h) \\ \sigma_{xy}(-h) \end{bmatrix} = \begin{bmatrix} 0 \\ 0 \\ 0 \\ 0 \end{bmatrix} = \begin{bmatrix} ae^{+i\gamma_p h} & ae^{-i\gamma_p h} & -be^{+i\gamma_s h} & be^{-i\gamma_s h} \\ ce^{+i\gamma_p h} & -ce^{-i\gamma_p h} & ae^{+i\gamma_s h} & ae^{-i\gamma_s h} \\ ae^{-i\gamma_p h} & ae^{+i\gamma_p h} & -be^{-i\gamma_s h} & be^{+i\gamma_s h} \\ ce^{-i\gamma_p h} & -ce^{+i\gamma_p h} & ae^{-i\gamma_s h} & ae^{+i\gamma_s h} \end{bmatrix} \begin{bmatrix} D_p \\ U_p \\ D_s \\ U_s \end{bmatrix}, \tag{8}$$

where $a = G(\beta^2 - \gamma_s^2)$, $b = 2G\beta\gamma_s$, and $c = 2G\beta\gamma_p$ are introduced for compactness. With a priori knowledge about the solution or by close consideration, one can see that there is a good match between the first two columns, as well as the last two. Therefore, instead of solving for the up- and down-going wave components, a solution to their combinations is sought:

$$\begin{bmatrix} 0 \\ 0 \\ 0 \\ 0 \end{bmatrix} = \begin{bmatrix} +a\cos(\gamma_p h) & +ai\sin(\gamma_p h) & -ib\sin(\gamma_s h) & -b\cos(\gamma_s h) \\ +ci\sin(\gamma_p h) & +c\cos(\gamma_p h) & +a\cos(\gamma_s h) & +ai\sin(\gamma_s h) \\ +a\cos(\gamma_p h) & -ai\sin(\gamma_p h) & +ib\sin(\gamma_s h) & -b\cos(\gamma_s h) \\ -ci\sin(\gamma_p h) & +c\cos(\gamma_p h) & +a\cos(\gamma_s h) & -ai\sin(\gamma_s h) \end{bmatrix} \begin{bmatrix} D_p + U_p \\ D_p - U_p \\ D_s + U_s \\ D_s - U_s \end{bmatrix}. \tag{9}$$

Then the following substitutions are performed $D_p + U_p \to A_2$, $D_p - U_p \to A_1$, $D_s + U_s \to B_2$, and $D_s - U_s \to B_1$. The potentials in Eq. (4) can thus be rewritten as

$$\phi = \left[A_2\cos(\gamma_p y) + iA_1\sin(\gamma_p y)\right]e^{i(\omega t - \beta x)}, \tag{10a}$$

$$\psi = \left[B_2\cos(\gamma_s y) + iB_1\sin(\gamma_s y)\right]e^{i(\omega t - \beta x)}. \tag{10b}$$

The substitutions will take on a more significant meaning soon, as they explain the symmetric and antisymmetric modes in the final solution.

The final step is to further simplify the matrix by row operations on row 1 and 3 and row 2 and 4:

$$\begin{bmatrix} 0 \\ 0 \\ 0 \\ 0 \end{bmatrix} = \begin{bmatrix} a\cos(\gamma_p h) & 0 & 0 & -b\cos(\gamma_s h) \\ ci\sin(\gamma_p h) & 0 & 0 & ai\sin(\gamma_s h) \\ 0 & -ai\sin(\gamma_p h) & +ib\sin(\gamma_s h) & 0 \\ 0 & c\cos(\gamma_p h) & a\cos(\gamma_s h) & 0 \end{bmatrix} \begin{bmatrix} A_2 \\ A_1 \\ B_2 \\ B_1 \end{bmatrix}. \tag{11}$$

To have a wave that can exist without forcing, the matrix must have a determinant of 0. Otherwise, it would be invertible and a non-zero solution of the vector of unknowns could not exist. Writing out the determinant gives

$$\begin{aligned} &[a^2\cos(\gamma_p h)\sin(\gamma_s h) + bc\cos(\gamma_s h)\sin(\gamma_p h)] \\ \cdot&[a^2\cos(\gamma_s h)\sin(\gamma_p h) + bc\cos(\gamma_p h)\sin(\gamma_s h)] = 0. \end{aligned} \tag{12}$$

The determinant is also the product of two individual 2-by-2 determinants in the two upper and two bottom rows. Each can be equal to 0 on its own, as seen from the two square brackets. It will be shown that the two brackets are associated with the symmetric and antisymmetric modes.

After choosing the material parameters and thickness for the plate, the two remaining unknowns are frequency and wavenumber. The two can be matched to give the dispersion relation $\omega(\beta)$ by solving for the zeros of a transcendental characteristic equation (one of the two brackets), a method for which is presented later. The wavefields in the plate can be described entirely once the dispersion relation is known.

ISBN 978-82-8123-021-7

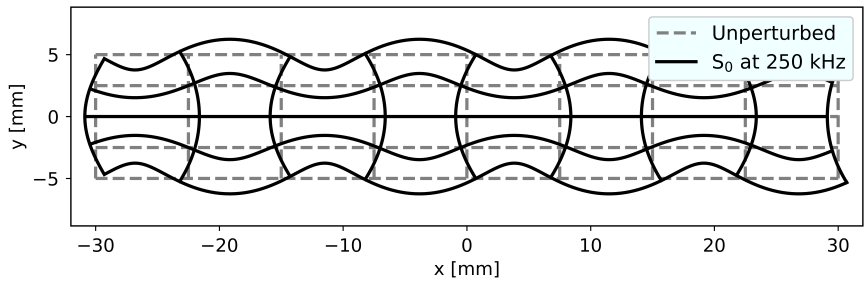

Figure 4: Displacement field of the S_0 mode at 250 kHz in a 1 cm thick steel plate.

2.1.1 Symmetric solution

When the first part of the characteristic equation (12), which describes the components A_2 and B_1, is set to zero, the dispersion relation is implicit in

$$\frac{\tan(\gamma_s h)}{\tan(\gamma_p h)} + \frac{4\beta^2\gamma_s\gamma_p}{(\beta^2-\gamma_s^2)^2} = 0. \tag{13}$$

To obtain the dispersion relation in practice, the roots of Eq. (13) have to be found numerically.

When the dispersion relation holds, the corresponding 2-by-2 submatrix in Eq. (11) has a determinant of 0, and therefore also a free row. That makes it possible to express the ratio of A_2 and B_1 as

$$R_S = \frac{B_1}{A_2} = \frac{(\beta^2-\gamma_s^2)\cos(\gamma_p h)}{2\beta\gamma_s\cos(\gamma_s h)}. \tag{14}$$

The potentials ϕ and ψ are then known, with the exception of an arbitrary scaling that will be represented by K. Substitution back into the relationships (3) and (6) give the full field equations for symmetric Lamb waves

$$\phi^S = K\cos(\gamma_p y) \tag{15a}$$
$$\psi^S = iKR_S\sin(\gamma_s y) \tag{15b}$$
$$v_x^S = i\omega K[\beta\cos(\gamma_p y) - \gamma_s R_S\cos(\gamma_s y)] \tag{15c}$$
$$v_y^S = \omega K[\gamma_p\sin(\gamma_p y) + \beta R_S\sin(\gamma_s y)] \tag{15d}$$
$$\sigma_{xx}^S = iGK[(2\gamma_p^2-\beta^2-\gamma_s^2)\cos(\gamma_p y) + 2\gamma_s\beta R_S\cos(\gamma_s y)] \tag{15e}$$
$$\sigma_{xy}^S = -GK[2\beta\gamma_p\sin(\gamma_p y) + (\beta^2-\gamma_s^2)R_S\sin(\gamma_s y)] \tag{15f}$$
$$\sigma_{yy}^S = iGK[(\beta^2-\gamma_s^2)\cos(\gamma_p y) - 2\gamma_s\beta R_S\cos(\gamma_s y)] \tag{15g}$$

Note that the displacements have been converted to velocities by multiplication with $i\omega$. The common phasor $e^{i(\omega t-\beta x)}$ is also omitted from all quantities.

The notion of symmetric waves come from the field equations. The x-velocities v_x are symmetric around the mid-plane of the plate if described by cosines as seen in Eq. (15c), whereas the y-velocity v_y is symmetric if described by sines as seen in Eq. (15d). For antisymmetric modes, the sines and cosines are swapped. The displacement field of an S_0 symmetric Lamb wave is shown in Fig. 4.

ISBN 978-82-8123-021-7

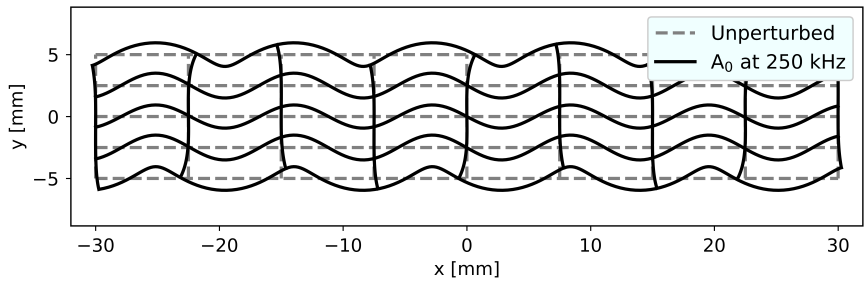

Figure 5: Displacement field of the A_0 mode at 250 kHz in a 1 cm thick steel plate.

2.1.2 Antisymmetric solution

The second part of the characteristic equation (12) describes the antisymmetric modes, and the dispersion relation is implicit in

$$\frac{\tan(\gamma_p h)}{\tan(\gamma_s h)} + \frac{4\beta^2\gamma_s\gamma_p}{(\beta^2-\gamma_s^2)^2} = 0. \tag{16}$$

The same steps as for the symmetric solution are followed. When the dispersion relation holds, the corresponding 2-by-2 submatrix in Eq. (11) has a free row since the determinant is 0. That makes it possible to express the ratio of A_1 and B_2 as

$$R_A = \frac{B_2}{A_1} = \frac{(\beta^2-\gamma_s^2)\sin(\gamma_p h)}{2\beta\gamma_s \sin(\gamma_s h)}. \tag{17a}$$

With the potentials known, again with the exception of an arbitrary scaling K, substitution back into the relationships (3) and (6) gives the full field equations for antisymmetric Lamb waves. Examples of the displacement fields of the A_0 and A_1 modes at 250 kHz are given in Fig. 5 and 6.

$$\phi^A = iK\sin(\gamma_p y) \tag{18a}$$
$$\psi^A = KR_A\cos(\gamma_s y) \tag{18b}$$
$$v_x^A = i\omega K[\beta\sin(\gamma_p y) - \gamma_s R_A \sin(\gamma_s y)] \tag{18c}$$
$$v_y^A = -\omega K[\gamma_p\cos(\gamma_p y) + \beta R_A\cos(\gamma_s y)] \tag{18d}$$
$$\sigma_{xx}^A = KGi[(2\gamma_p^2 - \beta^2 - \gamma_s^2)\sin(\gamma_p y) + 2R_A\beta\gamma_s\sin(\gamma_s y)] \tag{18e}$$
$$\sigma_{xy}^A = KG[2\beta\gamma_p\cos(\gamma_p y) + R_A(\beta^2-\gamma_s^2)\cos(\gamma_s y)] \tag{18f}$$
$$\sigma_{yy}^A = iKG[(\beta^2-\gamma_s^2)\sin(\gamma_p y) - 2R_A\beta\gamma_s\sin(\gamma_s y)] \tag{18g}$$

2.2 Lamb wave attenuation in light fluids

The Lamb wave derivation assume a free plate in vacuum. The interaction with a surrounding fluid or solid would need to be included already in the boundary conditions in Eq. (8). However, in situations where the plate is much denser than the surrounding material, as with a steel plate in water, the Lamb wave structure can be assumed to be unperturbed except for the addition of an imaginary attenuation term α to the wavenumber:

$$k_x = k_{xr} + ik_{xi} = \beta - i\alpha. \tag{19}$$

ISBN 978-82-8123-021-7

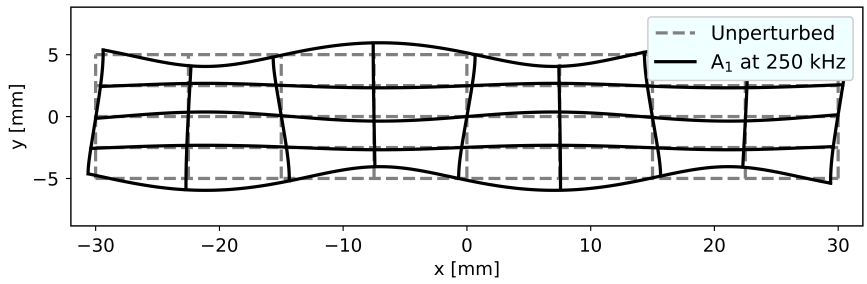

Figure 6: Displacement field of the A_1 mode at 250 kHz in a 1 cm thick steel plate.

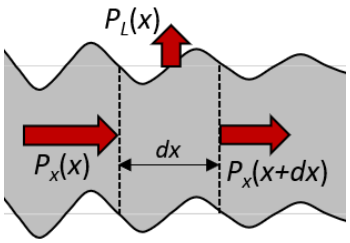

Figure 7: Balance of energy flow into a small element of a plate.

For a wave of initial amplitude A, this implies exponential decay with distance as

$$Ae^{i(\omega t - k_x x)} = Ae^{-\alpha x} \cdot e^{i(\omega t - \beta x)}, \tag{20}$$

with an the attenuation α often measured in neper per meter (Np/m), or in decibel $8.686 \cdot \alpha$ (dB/m).

Several perturbation techniques can be used to calculate approximate attenuation curves. Merkulov [9] used Schoch's characteristic equation (a generalization of Eq. (13) and (16) to include the effect of two-sided fluid loading) to come to an approximation of the attenuation by doing a first order perturbation and assuming the density of the fluid to be small. Another perturbation method is presented by Auld [10], starting from a complex reciprocity relation. The same numerical attenuation values are obtained with both methods through different equations. Here we will look a at a more intuitive method presented in 1982 by Watkins et al. [11] that leads to the same equations as Auld's method.

The main assumption is that the wave retains its structure although power is lost. Consider a differential element of the plate of unit depth, as illustrated in Fig. 7. In steady state a time averaged power $P_x(x)$ is incident from the left, and a power $P_x(x+dx)$ leaves from the right. On the top of the plate a total time-averaged power $P_L(x) = I_L(x) \cdot dx$ is lost to the medium through radiation. Conservation of energy requires that

$$P_x(x+dx) - P_x(x) = -I_L(x) \cdot dx \quad \longrightarrow \quad \frac{dP_x(x)}{dx} = -I_L(x). \tag{21}$$

The time-averaged power flow along the plate can be calculated as

$$P_x = -\frac{1}{2}\int_{-h}^{h} (v_x \sigma_{xx}^* + v_y \sigma_{xy}^*) dy. \tag{22}$$

The next step is to calculate the radiated intensity I_L. Here we only look at the case where the plate is in contact with a fluid, but it is similarly possible to calculate radiated intensity into a solid by taking into account how the vertical and horizontal velocity components contribute to radiated P- and S-waves. For fluids it is enough to consider that

ISBN 978-82-8123-021-7

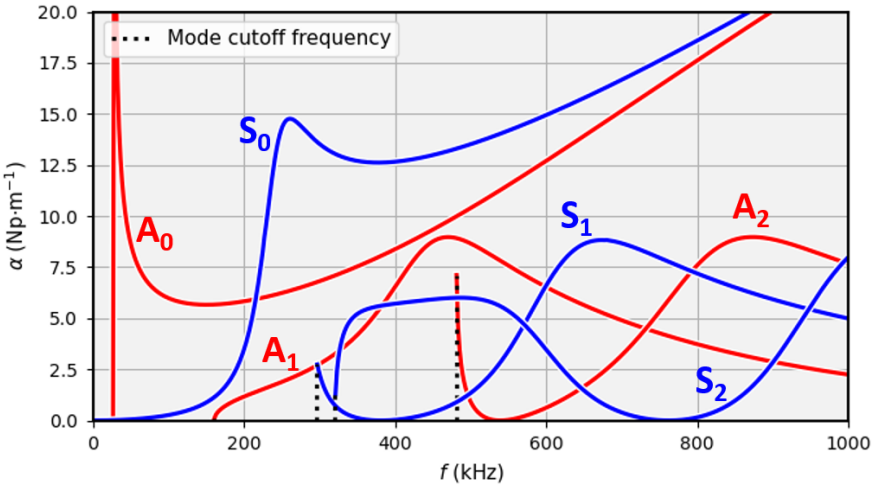

Figure 8: Perturbation values of attenuation for Lamb waves in a 1 cm thick steel plate in contact with water on both sides. Only the first three S- and A-modes are shown. The black dotted lines indicate cutoff frequencies.

the normal velocity is continuous on the interface, and related to the pressure through Euler's equation. The radiated intensity on one side of the plate is [12]

$$I_L = \frac{Z_f |\bar{v}_{ys}|^2}{\sqrt{1 - \left(\frac{c_f}{c_{ph}}\right)^2}}, \tag{23}$$

where $\bar{v}_{ys}$ is the RMS-value of the vertical velocity at the surface of the plate in contact with the fluid. c_f is the speed of sound in the fluid, and Z_f is the specific acoustic impedance, for water $Z_f = 1.48\,\text{MRayl}$.

The intensity and power flow both scale with the square of the amplitude. Hence, $I_L \propto P_x$, and the power flow and radiated intensity exponentially damped as e.g.

$$P_x(x) = P_x(0)e^{-2\alpha x}. \tag{24}$$

This can be inserted into Eq. (21), which can then be re-expressed as

$$\alpha = \frac{I_L}{2P_x} = \frac{\text{Power lost per metre into medium}}{2 \times \text{Power flow along the plate}}. \tag{25}$$

By knowing the dispersion relation, Eq. (22) can be integrated numerically, and Eq. (23) can be evaluated with the same arbitrary scaling K. The result for a steel plate in water is shown in Fig. 8. The curves are identical to Merkulov's first order approximation, but the power flow method benefits by being easier to understand and more flexible; it can treat radiation into solids, and preliminary findings [13] suggest that one can use inhomogeneous ("damped") waves [14] to partially correct for the singularity at coincidence (spike in A_0 mode) and the absence of subsonic radiation. Around coincidence, the real wavenumber also changes appreciably, but the physics get more complicated at lower frequencies, and the current scope is on the higher frequencies. Note that the attenuation curves can deviate significantly from the perturbation solution at higher frequencies if the plate is in contact with water on only one side, or if the fluids have different impedance.

For the purposes of this work, it is more suitable to define the attenuation as happening in time. If ω is taken to be real, the imaginary wavenumber gives a complex

ISBN 978-82-8123-021-7

propagation speed $c = c_r + ic_i$, where $c_r \neq c_{ph}$. To achieve the same attenuation within time interval Δt as with α over the distance $\Delta x = c_{ph}\Delta t$, one can add an imaginary part $i\omega_i$ to ω,

$$Ae^{-\alpha\cdot\Delta x} = Ae^{i\cdot i\omega_i\cdot\Delta t} \quad \longrightarrow \quad \omega_i = \alpha\frac{\Delta x}{\Delta t} = \alpha c_{ph} = \frac{\alpha}{\beta}\omega, \tag{26}$$

and discard the imaginary part of the wavenumber.

2.3 The angular spectrum approach

The angular spectrum method is a superposition method for modeling the propagation of a wave field when the solution is supplied on the plane $y = y'$ [12]. It is based on the fact that $e^{i(\omega t - \boldsymbol{k}\cdot\boldsymbol{r})}$ is a solution of the Helmholtz equation

$$\nabla^2 p + k^2 p = 0, \tag{27}$$

when the wave vector components satisfy

$$k^2 = k_x^2 + k_y^2 + k_z^2 = \beta^2 + k_y^2 = \frac{\omega^2}{c^2}. \tag{28}$$

Note that the wavenumber along an arbitrary propagation direction in the waveguide is given by $\beta^2 = k_x^2 + k_z^2$. Since k is constant for each frequency, the three wavenumbers are not independent. Choosing k_y as dependent, one has that $k_y = \pm\sqrt{k^2 - k_x^2 - k_z^2}$, where the appropriate root must be chosen.

When a vibrating steel plate is in contact with e.g. air, the wavefield in the x-z plane is given because it is imposed by the velocity field of the steel plate. The traces of the wavefronts in the air must match the wavefronts on the steel. The component k_y can thus be real or imaginary as a consequence. The latter implies a non-propagating evanescent wave into the air, when the phase velocity of the plate wave is subsonic with respect to the surrounding air.

First consider an initial complex wavefield at $t = 0$ on the plate surface at $y = y'$, expressed through its vertical surface velocity v_{ys}. It can be decomposed into a sum of plane waves through the Fourier transform

$$V_{ys}(k_x, k_z) = \mathcal{F}_x\mathcal{F}_z\{v_{ys}(t = 0, x, y = y', z)\}, \tag{29}$$

which is also known as the angular spectrum. For waves propagating on a plate, the dispersion relation $\omega(\beta)$ is already known, and using Eq. (26), the attenuation with time can be included.

The time-evolution of each plane wave component has a simple description, only changing by a phase factor and attenuated. Therefore, the propagated wavefield on the plate can be obtained by injecting a "time propagator", and performing the inverse Fourier transform:

$$v_{ys}(t, x, y = y', z) = \iint \underbrace{V_{ys}(k_x, k_z)}_{\text{Angular spectrum}} \cdot \overbrace{e^{i(k_x x + k_z z)}}^{\text{Fourier Basis}} \cdot \underbrace{e^{i(\omega(\beta) + i\omega_i)t}}_{\substack{\text{Time}\\ \text{propagator}}} dk_x dk_z. \tag{30}$$

The normal velocity field is interesting on a plate, but the pressure p is more meaningful in a fluid. Euler's equation in the frequency domain can be used to relate the normal velocity to the fluid pressure just above the plate

$$i\omega\rho\boldsymbol{V} = -\nabla P. \tag{31}$$

ISBN 978-82-8123-021-7

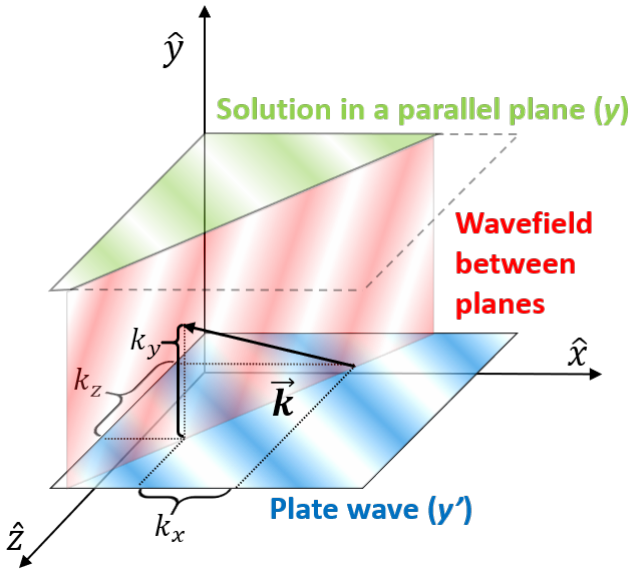

Figure 9: Propagation of a monochromatic wavefield from a plate (blue) into a parallel plane (green). The colored gradients represent wavefronts. The wave vector components k_x and k_z are imposed by the plate at $y = y'$. The wavefield between the planes, here shown as a cross section (red), can be calculated as different solution planes.

Doing the conversion using the dispersion relation frequency $\omega(\beta)$ brings some benefits that will be discussed in section 3.3. In that case one can calculate the angular spectrum of the pressure field above the plate at $t = 0$, $P(k_x, k_z)$. Then, it is possible using the method represented in Eq. (30) to propagate the wavefield to different times of interest, giving $P(t, k_x, k_z)$. Performing a Fourier transform over the t-dimension, one obtains $P(\omega', k_x, k_z)$, with ω' given by the sampling of t, and not the dispersion relation. Since k_y in the fluid is given by k_x and k_z via Eq. (28), one can propagate the wavefield between parallel planes, as shown in Fig. 9, as

$$p(t,x,y,z) = \iiint \underbrace{P(\omega', k_x, k_z)}_{\text{Angular spectrum}} \cdot \overbrace{e^{i(\omega' t + k_x x + k_z z)}}^{\text{Fourier Basis}} \cdot \underbrace{e^{ik_y(y'-y)}}_{\substack{\text{Propagator to} \\ \text{parallel planes}}} dk_x dk_z d\omega'. \tag{32}$$

In practice, the implementation uses the Fast Fourier Transform (FFT) or its inverse (IFFT). Hence, the solution domain will have to be sampled to resolve the shortest wavelength and highest frequency, and it will be periodic. The method naturally handles effects such as diffraction, dispersion, and attenuation.

Another method known as normal mode expansion (NME) [6, 15] is similar in some aspects to the presented method. It is a method for calculating the excitation of waveguides, and works by computing "modal participation factors" that carry a similar meaning to the angular spectrum coefficients here.

3 Method

3.1 Numerical solution of the Lamb dispersion relation

Equations (13) and (16) implicitly relate the frequency ω to a wavenumber β along the propagation direction. For any frequency, there are a finite number of purely propagating

ISBN 978-82-8123-021-7

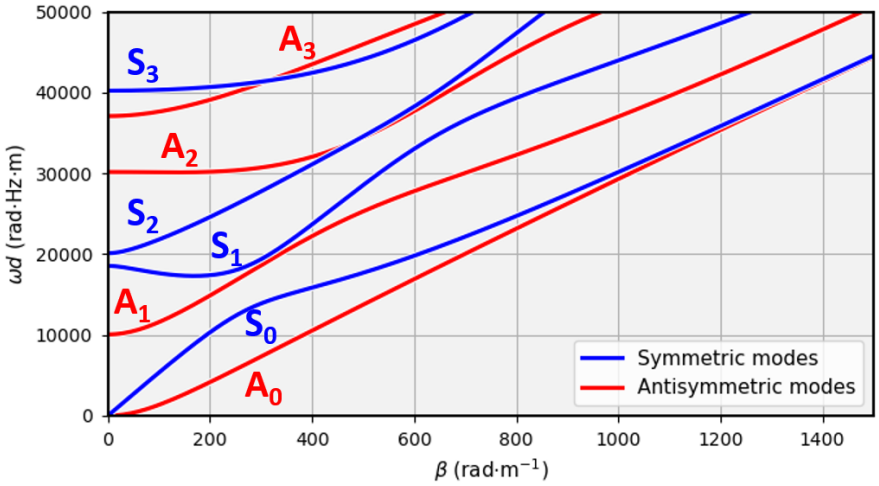

Figure 10: Dispersion curves as they are traced out. Notice that the curves are not one-to-one, and more predictable than e.g. the phase velocity Fig. 2.

modes (A_0, S_0, A_1, S_1, etc.), as shown e.g. in Fig. 2. Tracing out the dispersion curves is necessary, and this section describes a procedure to do so.

The first step is to recognize that γ_s and γ_p will change from being real to imaginary depending on the wavenumber β and frequency. This causes (13) and (16) to switch between having real and imaginary roots. As an example of a special case, it is known that the phase velocity for the A_0 mode is bounded between 0 and the Rayleigh wave velocity $c_R < c_s$, making the vertical wavenumbers γ_s and γ_p imaginary. For other modes, one or both of the vertical wavenumbers may become real at some point. To simplify analysis, it is therefore useful to rewrite the characteristic equations so they take on only real values for real horizontal wavenumbers β. From Rose [6], this can be done as

$$\frac{\tan(\gamma_s h)}{\gamma_s} + \frac{4\beta^2\gamma_p \tan(\gamma_p h)}{(\gamma_s^2 - \beta^2)^2} = 0 \quad \text{for symmetric modes,} \tag{33a}$$

$$\gamma_s \tan(\gamma_s h) + \frac{(\gamma_s^2 - \beta^2)^2 \tan(\gamma_p h)}{4\beta^2\gamma_p} = 0 \quad \text{for antisymmetric modes.} \tag{33b}$$

The curves change sign when crossing 0, so a root-finding algorithm can be used. However, caution should be taken as the equations also change sign when crossing a pole. Depending on the algorithm used, one should test that the obtained root is in fact fairly close to 0. The curves are traced out as $\omega(\beta)$, as seen in Fig. 10 for two reasons. Firstly, these curves are two-to-one, meaning we can capture the back-propagating modes (negative group velocity, e.g. S_1 mode at low frequencies). Secondly, as Lowe points out [1], they are more easily traced out than say $c_{ph}(\omega)$ which perhaps is the most intuitive choice to go for.

Tracing out the modes is a bit involved, in particular due to the possibility of having holes in the curves. The holes are regions where no roots are found for a mode, and the consequences are potentially that a mode is missed, or that one reaches a dead end when following a curve. In brief, the algorithm used here works as follows:

1. Choose either Eq. (33a) or (33b).

ISBN 978-82-8123-021-7

2. Make a list of β values: $(\beta_0, \ldots, \beta_i, \beta_{i+1} \ldots \beta_n)$ for a fine search for roots/modes along the ω axis.

3. For each β_i, trace out the modes found as follows:

   i Store the values of each root as the intersection with a mode.

   ii Do a similar search nearby $(\beta_i + \delta\beta)$ to estimate the derivative $\partial\omega/\partial\beta$.

   iii Trace the modes (as far as possible) down to β_{i-1} and up to β_{i+1}, taking small steps of e.g. $\Delta\beta = 5$, and store the result as a piece of a mode curve for the index i.

4. Starting from $i = 0$, go through each curve piece, and splice with the best matching curve piece in $i = 1$ (if any), then for $i = 2$, and so on:

   i Splice two curve pieces if they overlap at some point with a similar angle (< 5 degrees).

   ii If any curve pieces remain, they are attempted to be matched based on how well linear extrapolation finds the midpoint between the unconnected ends. An upper tolerable error is defined from the derivatives $\partial\omega/\partial\beta$, and length of the gap.

   iii Unmatched curve pieces are at this point considered as new modes.

5. The fully traced modes are then labeled e.g. A_0, A_1, etc. based on their lowest frequency, in line with how higher modes have higher cut-off frequencies [16].

6. The mode curves are finally fitted with a spline function to get $\omega(\beta)$. For the inverse function $\beta(\omega)$ the fit ignores the back-propagating modes, so it is a one-to-one function.

When a spline function is obtained, it is quite easy and fast to work with, as the mode tracing is separate from everything else. The method above has worked very well for steel plates and similar materials up to at least 1 MHz·mm, but for very different material parameters it is difficult to assess general robustness. Using the above method will therefore require inspection, and potential tweaking of hyperparameters such as the step length $\Delta\beta$. It should also be mentioned that at very low frequencies, the A_0 and S_0 modes may be difficult to trace due to issues relating to the numerical range and precision of e.g. floats or doubles in the characteristic equations. In those situations, the low frequency approximations given in [16] can be used. Finally, in cases where one is interested in general leaky Lamb dispersion relations, the wavenumber is complex, and the search for roots is significantly more difficult, but still possible as described by Lowe [1].

3.2 Plate wave propagation

To propagate a wavefield on a plate, the first step is to choose the dimensions and discretization of the plate. The Nyquist sampling theorem requires more than two samples per smallest wavelength to be simulated. Then, the vertical surface velocity v_{ys} profile is specified, and here we will consider the simple case of a Gaussian wavepacket propagating along the x-direction, $\theta = 0$, on the plate. It can be expressed as

$$v_{ys}(t = 0, x, z) = e^{-\frac{(x-x_0)^2+(z-z_0)^2}{2\sigma^2}} \cdot e^{-i\beta_c[\cos\theta(x-x_0)+\sin\theta(z-z_0)]}, \tag{34}$$

ISBN 978-82-8123-021-7

where β_c is the wavenumber at the center frequency of the wavepacket, and x_0 and z_0 the initial location. The wavefield is complex valued, which is necessary for defining the propagation direction. The spatial extent of the wavepacket is given by σ^2, using the full width at half maximum (FWHM), $\sigma \approx \text{FWHM}/2.355$. In this work $\text{FWHM} = 2\lambda_c = 4\pi/\beta_c$.

An attractive feature of the method is that specifying only v_{ys} is enough, even though one has velocity components in the x-direction, and stress/strain fields inside the plate. The reason is that all field relations are implicit in the Lamb wave assumption and dispersion relation. The only situation where v_{ys} cannot capture a Lamb wave mode, is for certain frequencies in the higher modes. Looking at Fig. 8, the S_1 mode has 0 attenuation at a particular frequency, and the reason is that $v_{ys} = 0$ even though there is a wave with non-zero power flow P_x. For each Lamb mode the procedure of calculating propagation is:

1. **Starting point:** Complex wavefield or wavepacket at $t = 0$, (x, z).
2. **Fourier transform:** Wavenumber domain, (k_x, k_z).
3. **Propagate to different times:** Using the "time propagator" in Eq. (30), (t, k_x, k_z).
4. **Inverse Fourier transform:** Propagated wavefields, (t, x, z).

The parenthesis at each step shows the the dimensions of the data worked with. A reason why the method is fast is that optimized FFT routines can be used, along with broadcasting/vectorization. Using Python, the step from (k_x, k_z) to (t, k_x, k_z) is written on one line using Numpy arrays, completely avoiding inefficient Python loops.

Table 1: Material parameters used.

Material	ρ (kg·m^{-3})	c_p (m·s^{-1})	c_s (m·s^{-1})
Steel	7850	5900	3200
Water	1000	1480	-

3.3 Including leakage to fluid

Sometimes a plate wave can be interesting to model on its own, but in most practical settings the interaction with a surrounding fluid is key. A few modifications to the list in the previous section is needed; new steps are marked with (*):

1. **Starting point:** Complex wavefield or wavepacket at $t = 0$, (x, z).
2. **Fourier transform:** Wavenumber domain, (k_x, k_z).
3. *** Convert to pressure:** Using Euler's equation (alternatively after step 6).
4. *** Add attenuation:** $\omega \to \omega(1 + i\frac{\alpha}{\beta})$.
5. **Propagate to different times:** Using the "time propagator", (t, k_x, k_z).
6. *** Transform to frequency domain:** ω' given by sampling of t, (ω', k_x, k_z).

ISBN 978-82-8123-021-7

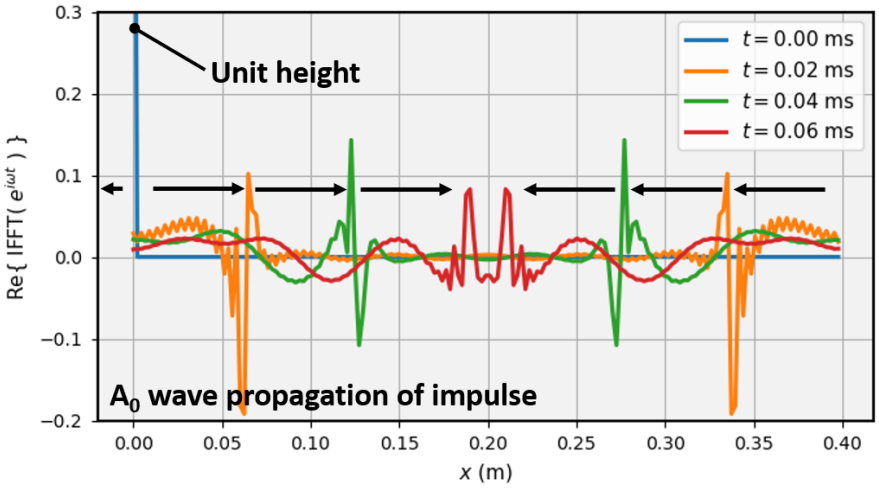

Figure 11: The equivalent convolution kernels that propagates a wavefield as a leaky A_0 Lamb wave by a time t.

i If step 3 is moved, reduce spectral leakage from the "sudden" initialization of the plate wave with a window function in time, e.g. Tukey (see next section).

ii Zero padding to avoid temporal wrap-around with y (see next section).

7. * **Propagate to parallel planes of interest:** Using Eq. (32), (ω', k_x, y, k_z).

8. **Inverse Fourier transform:** Wavefield in fluid, (t, x, y, z).

Step 3, converting to pressure, can alternatively be moved to after step 6. The difference is between using the frequency from the dispersion relation ω, or the frequency from the time sampling t, ω'. Doing the conversion in step 3 with ω avoids an unwanted "startup wave" as in Fig. 16.

3.4 Frequency domain periodicity

The method works in the frequency domain where the solution is periodic. To understand the implications of that, we start by looking at the "time propagator" in more detail. It works like a filter that is applied in the frequency domain by multiplication. In the spatial domain, it would be a convolution by a kernel that is a function of propagation time, as shown in Fig. 11.

The intial impulse splits into a left- and right-going pulse. Which direction is determined by the wavenumber, so if the initialized wavefield is defined to move to the right, the left-going pulse will be zero. The peak in this particular case moves at roughly the typical group velocity (A_0 mode), and attenuation is included. Once the pulse moves to the right end ($x = 0.4$ m) it will wrap back to the beginning ($x = 0.0$ m).

To avoid wraparound effects, one must essentially the avoid the effects of circular convolution that may turn up when doing the convolution in the frequency domain without zero-padding. To have linear convolution, the length L after convolution must be given by

$$L = N + M(t) - 1, \tag{35}$$

where N is the number of samples in the domain, and $M(t)$ is the appropriate number of samples in the convolution kernel. In the circular convolution case $L = N$, and $M(t)$

ISBN 978-82-8123-021-7

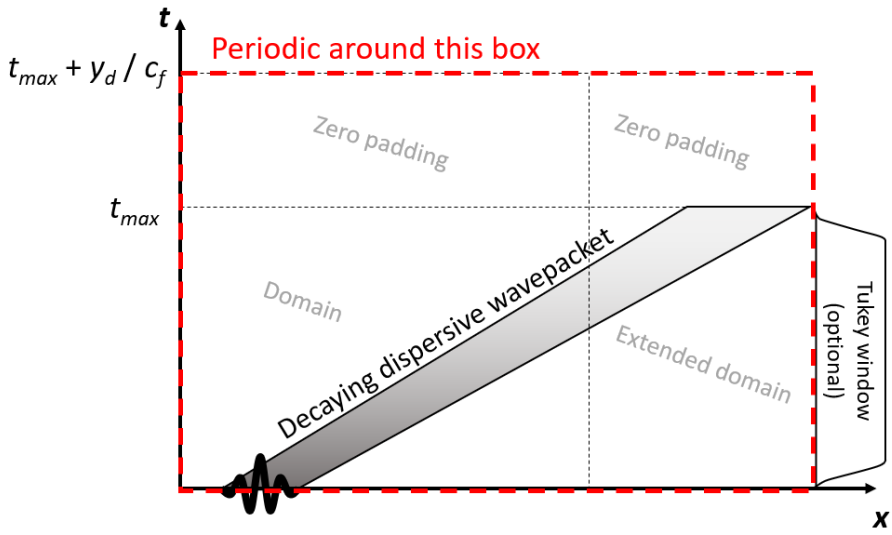

Figure 12: Illustrations of necessary domain extension and zero padding in time to avoid wrap-around artifacts. The Tukey window is optional, but reduces spectral leakage if one does the conversion to pressure after step 6 in the recipe.

is then the zero-padding needed to extend the domain, see Fig. 12. It can be decided by taking into account the largest group velocity of interest, the propagation time, and the spatial sampling rate. It may not be necessary to use full domain extension if, for instance, the wavefield consists of a well localized wavepacket on one side of the domain.

When the wavefield of the plate is propagated into the fluid, the propagation delay plays a role. The wavefield a distance y_d away from the plate surface is unaffected by the current plate vibration until a time $t_d = y_d/c_f$ has passed, depending on the sound speed in the fluid c_f. From step 6 in the recipe in sec. 3.3, the solution is periodic in time, and when moving away from the radiating plate surface, the wavefield is determined by a increasingly distant past. Therefore, as the distance y increases, the delayed time will eventually cause a wrap-around in the solution. To avoid this, sufficient zero padding in time must be used. The amount depends on how far away from the plate one wants to propagate the wavefield. A schematic representation of necessary zero padding is shown in Fig. 12.

4 Results and discussion

4.1 Free plate propagation

The method is implemented in Python, and compared with equivalent simulations in COMSOL Multiphysics. To verify 1D propagation for a free plate, an A_0 wavepacket propagating to the right is initialized at $x_0 = -25$ cm with a center frequency of 250 kHz. The vertical midplane velocity is measured.

The COMSOL simulation is realized by calculating the necessary fields $\boldsymbol{u}(x,y)$ and $v(x,y)$, using e.g. Eq. (18c), at the center frequency of 250 kHz, and windowing using a Gaussian function. This is an approximation, as the windowing introduces a bandwidth of frequencies that are not properly modeled. It is deemed unfeasible to synthesize the different fields one frequency at a time, but for this example, the maximum deviance in intensity I_x that contributes to the power flow P_x is 2%. For all simulations 6 quadratic

ISBN 978-82-8123-021-7

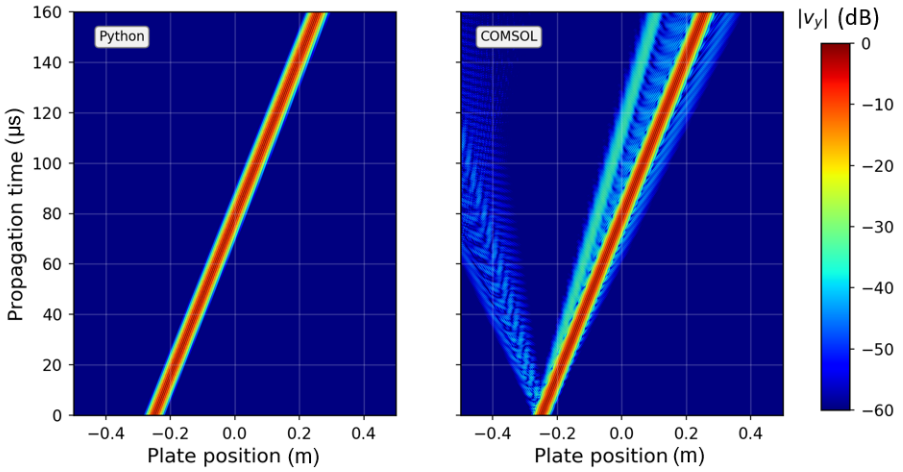

Figure 13: Comparison of 1D propagation for a free plate. The presented method is shown in the Python implementation. The COMSOL simulation shows additional modes due to the approximation used when initializing the fields.

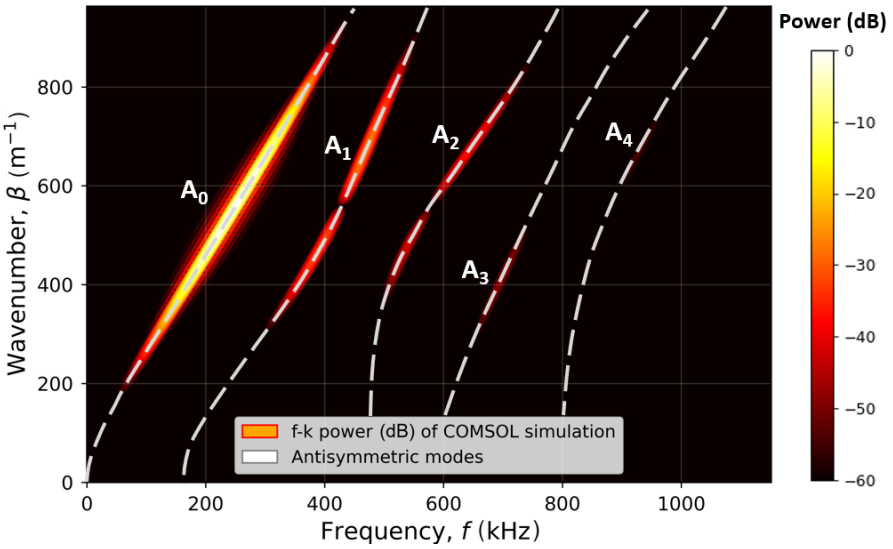

Figure 14: f-k plot from the COMSOL simulation between $-0.2\,\mathrm{m}$ to $0.3\,\mathrm{m}$ and from $20\,\mu\mathrm{s}$ to $140\,\mu\mathrm{s}$. The modes A_1, A_2 etc. come from the inexact initialization in COMSOL.

elements per wavelength at 500 kHz is used, unless stated otherwise.

The propagation in the two cases can be seen in Fig. 13. The method presented in this work shows a single very weakly dispersive wavepacket. In COMSOL, the targeted A_0 wavepacket is simulated in the same way, but additional modes are also present. The explanation is the approximation used when initializing the fields. The f-k plot in Fig. 14 shows clearly that the deviation comes from higher-order antisymmetric Lamb modes, confirming that the error is related to the initialization and not numerical.

A verification of 2D propagation is also shown in Fig. 15, where one sees the wavepacket from above the plate as it propagates and diffracts. The two different solutions are shown on each side of the symmetry axis. For the same reasons as in 1D, there are additional modes in this simulation, but it is quite clear that the main A_0 wavepacket behaves similarly. The boundary conditions at $z = \pm 0.1\,\mathrm{m}$ are different; they are periodic in the Python implementation, and fixed in COMSOL. The reason touches on the motivations

ISBN 978-82-8123-021-7

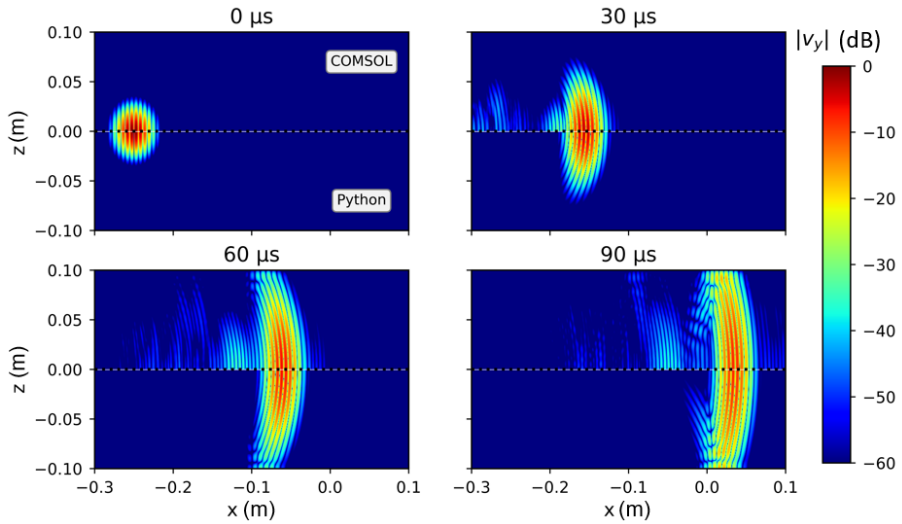

Figure 15: 2D propagation, with different solutions above and below the propagation axis. The x-z-plane represents the plate surface.

for the work, as a very fine mesh is needed for simulating ultrasonic waves. Also, the 2D propagation requires a 3D model to capture the plate thickness, and the memory usage and simulation time had to be reduced. Even when using two planes of symmetry, reducing the maximum frequency to 400 kHz, and shrinking down the domain into what is seen, it still took roughly 8 hours to compute. Although no formal benchmarking has been performed, the computation time on the same computer was on the order of a couple of seconds using the presented method.

4.2 Leaky wave propagation

Simulations of fluid interaction are performed in 1D. The setup consists of a steel plate of 1 cm thickness with water on both sides, as seen in Fig. 16. Here it is assumed that the Lamb waves do not change their propagation characteristics except for being attenuated.

The COMSOL simulation shows a “startup” wave that seem to spread almost circularly from the initial position. It is not seen in the vertical surface velocity, and is therefore not a form of interface wave, but an artifact that occurs when a wave suddenly “pops” into existence. The comparison is done by monitoring the pressure 1 cm above the plate, as illustrated with the red dotted line.

In this work, the artificial “startup” wave is not present, as seen in Fig. 17. The reason has already been discussed, and is attributed to the velocity to pressure conversion before propagating the wavefield in time. Doing the conversion to pressure at a later stage introduces the “startup” wave. A finer comparison of the waveforms 1 cm above the plate is shown in Fig. 18. As soon as the “startup” wave and the leaked wavefield separate after some time, it shows that both attenuation and wave shape is modeled quite well. A slight shift of the waveform is likely owing to the minor influence of the water loading on the exact real horizontal wavenumber β, and/or numerical dispersion in COMSOL.

ISBN 978-82-8123-021-7

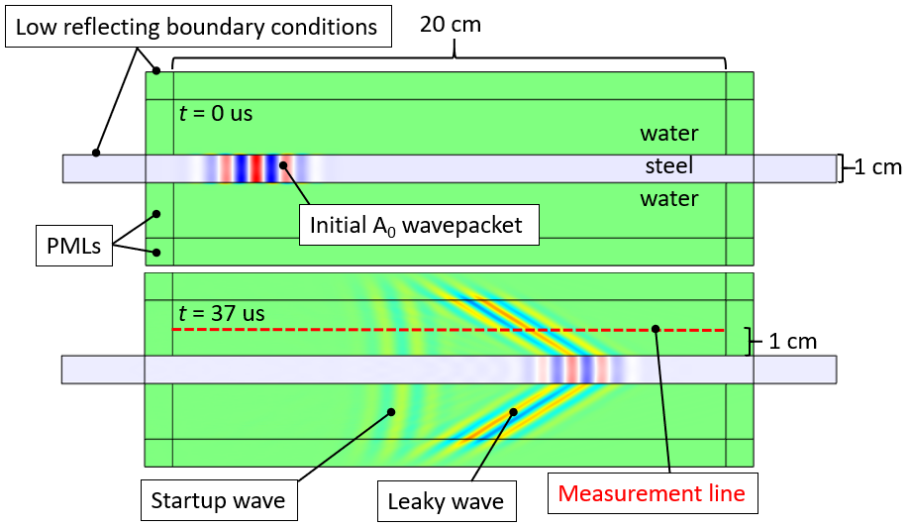

Figure 16: COMSOL model used to verify leaky wave propagation. The measurement line indicates the x-axis shown in Fig. 18.

5 Conclusion

A fast semi-analytical method that can propagate initialized leaky Lamb wavefields has been presented. Although no formal benchmarks have been performed, it is clear that computations are done within seconds, while matching computations in COMSOL have usually taken several hours. The speed-up is mainly attributed to

1. having precomputed the propagation characteristics in e.g. the dispersion relation,
2. not having to discretize the direction normal to the plate and having all field relations implicit, and
3. benefiting from optimized FFT routines and vectorization.

The method has been tested for A_0 wave propagation under the assumption that the fluid is sufficiently light compared to the plate so that classical Lamb wave theory together with a perturbative method for calculating attenuation is sufficient. The agreement is good, and assumed sufficient for most applications. Because the unwanted "startup" wave is not turning up in the presented method, it is well suited for calculating leaked wavefields in a fluid from known wavefields on a plate.

Acknowledgment

The contribution of E.M. Viggen to this work was supported by the Research Council of Norway under grant number 237887.

References

[1] M. J. S. Lowe, "Matrix techniques for modeling ultrasonic waves in multilayered media," *IEEE Transactions on Ultrasonics, Ferroelectrics, and Frequency Control*, vol. 42, no. 4, pp. 525–542, 1995.

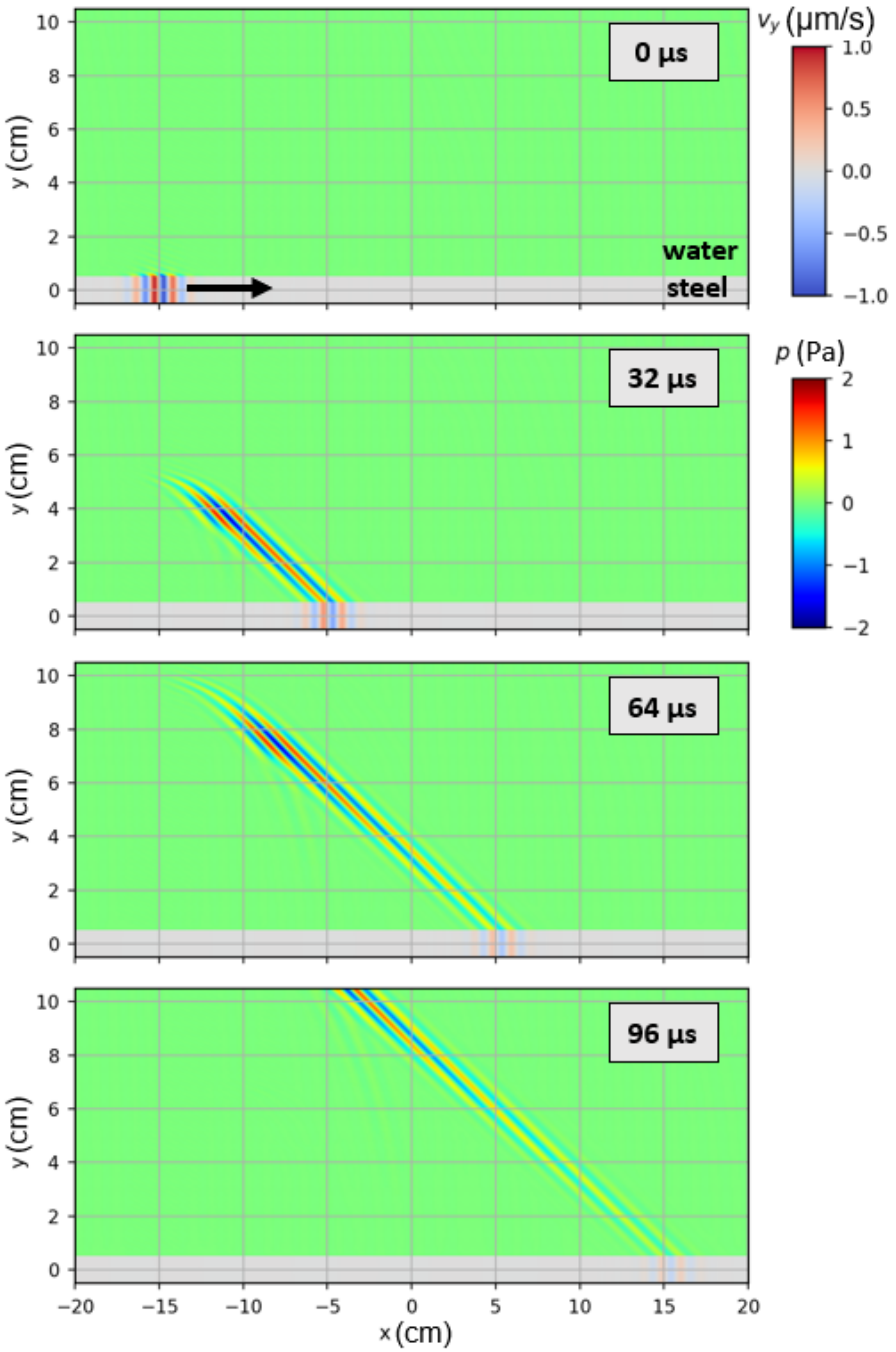

Figure 17: Sequence of snapshots from a simulation of an A_0 wavepacket on a steel plate in water, using the method presented in this work.

ISBN 978-82-8123-021-7

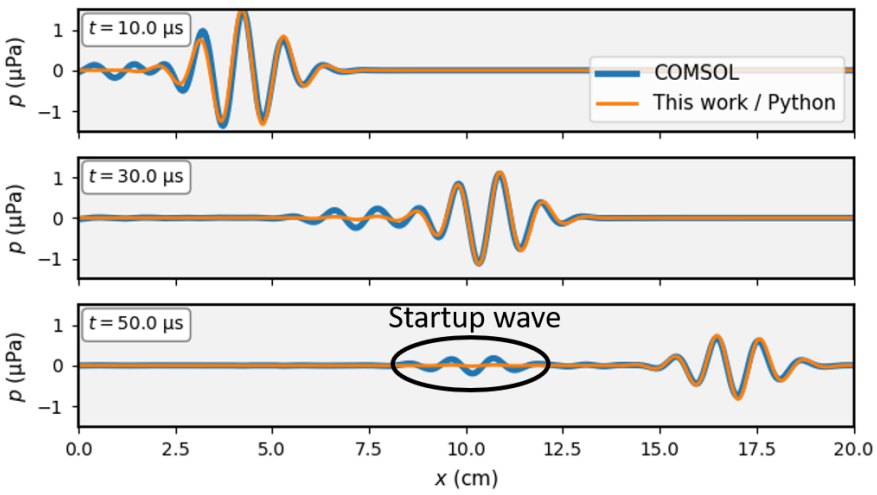

Figure 18: Comparison of this work with COMSOL. The biggest difference is the absence of the "startup wave" which is an artifact when a wavepacket suddenly comes into existence.

[2] R. van Kuijk, S. Zeroug, B. Froelich, M. Allouche, S. Bose, D. Miller, J.-L. le Calvez, V. Schoepf, and A. Pagnin, "A novel ultrasonic cased-hole imager for enhanced cement evaluation." Presented at the International Petroleum Technology Conference, 2005.

[3] C. Klieber, T. Brill, S. Catheline, Y. Vincensini, and F. Mege, "Visualization of Leaky Ultrasonic Lamb Wave Experiments in Multilayer Structures," *Physics Procedia*, vol. 70, pp. 314–317, 2015.

[4] E. M. Viggen, T. F. Johansen, and I.-A. Merciu, "Simulation and modeling of ultrasonic pitch-catch through-tubing logging," *Geophysics*, vol. 81, no. 4, pp. D383–D393, 2016.

[5] ——, "Simulation and inversion of ultrasonic pitch-catch through-tubing well logging with an array of receivers," *NDT & E International*, vol. 85, pp. 72 – 75, 2017.

[6] J. L. Rose, *Ultrasonic Guided Waves in Solid Media*. Cambridge University Press, 2014.

[7] J. Hovem, *Marine Acoustics: The Physics of Sound in Underwater Environments*. Peninsula Publishing, 2012.

[8] K. D. Lohne, P. Lunde, and M. Vestrheim, "Ultrasonic signal transmission in plates – study of a steel plate immersed in water," ser. Proceedings to the 31th Scandinavian Symposium on Physical Acoustics, 2008.

[9] L. G. Merkulov, "Damping of normal modes in a plate immersed in a liquid," *Soviet Physics-Acoustics*, vol. 10, no. 2, pp. 169–173, 1964.

[10] B. A. Auld, *Acoustic Fields and Waves in Solids*, 2nd ed., ser. Acoustic Fields and Waves in Solids. Krieger Publishing Company, 1990, vol. II.

[11] R. D. Watkins, W. H. B. Cooper, A. B. Gillespie, and R. B. Pike, "The attenuation of lamb waves in the presence of a fluid," *Ultrasonics*, vol. 20, no. 6, pp. 257 – 264, 1982.

ISBN 978-82-8123-021-7

[12] G. Williams, *Fourier Acoustics: Sound Radiation and Nearfield Acoustical Holography*. Elsevier Science, 1999.

[13] E. M. Viggen and H. K. Arnestad, "Understanding sound radiation from surface vibrations moving at subsonic speeds," in *Proceedings of the 44th Scandinavian Symposium on Physical Acoustics*. Norwegian Physical Society, 2021, p. 4, extended abstract.

[14] N. Declercq, R. Briers, J. Degrieck, and O. Leroy, "The history and properties of ultrasonic inhomogeneous waves," *IEEE transactions on ultrasonics, ferroelectrics, and frequency control*, vol. 52, pp. 776–91, 2005.

[15] A. M. Kamal, B. Lin, and V. Giurgiutiu, "Exact analytical modeling of power and energy for multimode lamb waves excited by piezoelectric wafer active sensors," *Journal of Intelligent Material Systems and Structures*, vol. 25, no. 4, pp. 452–471, 2014.

[16] I. A. Viktorov, *Rayleigh and Lamb Waves*. Plenum Press, 1967.

ISBN 978-82-8123-021-7